Distributed RSS-Based 2D Source Localization System in Extended Indoor Environment

**Tunguturi Sridher[1], Achanta D. Sarma[1, *],
Perumalla Naveen Kumar[2], and Kuruva Lakshmanna[1]**

Abstract—The evolution of computing and network technologies which involve thousands of devices that are connected wirelessly to serve variety of applications in Internet-of-Things (IoT) draws significant interest in locating the indoor objects. In our paper, we focuse on developing a hybrid source positioning technique with off-the-shelf hardware modules. A rectangular corridor with a multipath environment is considered in our work. For better localization accuracy, the corridor is classified into segments with threshold RSS values. Based on the measurement data, segment-wise logarithmic regression models are developed, and the performance in terms of Correlation Coefficient (R^2) and Root Mean Square Error (RMSE) is evaluated. For localization, basically trilateration is used. However, to overcome the adverse issues due to the indoor environment such as flip ambiguity, uncertainty in range measurements, circumscribing the circle's scenarios, two circle intersection, dynamic circle contraction, and expansion methods are used. Relevant Pseudocode algorithms are presented. The proposed hybrid method significantly improves the localization accuracy. The standard deviation of errors in x and y directions are about 16.75 cm, 66.24 cm in the first segment and 19.75 cm, 60.16 cm in the second segment. The analysis and results are useful in establishing state of the art IoT and future generation 5G networks.

1. INTRODUCTION

Radio Frequency (RF) propagation analysis in indoor environments is useful for localization applications. The latest trend in addressing localization is the use of off-the-shelf hardware transceiver modules. These modules are readily available at a low cost and can be easily configurable. Because of the growing demand due to several applications, there is a necessity to test the behavior of these modules in different environmental conditions. Therefore, estimation of coverage and capacity of these modules is very important in designing a wireless communication system. Nowadays indoor localization finds applications in many ways, including finding instore items, patients in hospital rooms, etc. In such instances, location is a critical input. To perform the localization, compared to the available techniques in literature such as Time of Arrival (TOA), Time Difference of Arrival (TDOA), or other angular techniques, Received Signal Strength (RSS) is an attractive approach since it does not require additional hardware for range estimation and time synchronization. In addition, most popular wireless technologies like Wi-Fi, ZigBee, RFID, and Bluetooth support the same type of RSS, TOA, and TDOA algorithms [1, 2]. RSS measurements are not an easy task in an indoor environment due to multipath, reflection, and refraction. With the best practices in range measurements, the errors in the RSS technique can be minimized. Such an improved approach is very helpful in radio planning also for future generation 5G networks.

Recently, [3] presented their work on 2.4, 5.3, 28, 60, and 73.5 GHz by developing an indoor path loss prediction model with incorporating wall correction factors and suggested that the developed model would be useful for planning wireless local area networks and also for 5G networks. In [4, 5], their joint RSS-based localization method addressed the problem of detecting the unknown target position in a distributed network in the presence of multiplicative fading, and low complexity fusion rules were developed to achieve good performance in detecting the target position. Also, their proposed Generalised version of the Rao test (G-Rao) was compared with the Generalised Likelihood-Ratio Test (GLRT) in terms of performance and computational complexity and proved an attractive alternative solution to GLRT in a distributed environment. [6] developed the cluster-based circle expansion algorithm by adjusting the estimated distances dynamically using the estimated distance from the strong signal module for improving the accuracy of trilateration. A similar type of work is also followed by [7] for improving the localization accuracy. In this paper, we focus on modeling the indoor corridor propagation path loss using the logarithmic regression and localization based on a segment-based circle contraction/expansion algorithm.

We used low-cost off-the-shelf hardware modules to acquire the RSS data from modules and used iterative procedure and bubble sorting algorithms to select the optimum RSS value to characterize the channel. Poor quality of trilateration problems, such as "flip ambiguity" and one circle circumscribing another circle, are critically analysed, discussed with reasons, and solved with hybrid localization method by following certain conditions.

This paper is organized as follows. Relevant theoretical background with a summary of various relevant trilateration scenarios is discussed in Section 2. Experimental setup, environment details, and technical properties of modules are covered in Section 3. The relation between RSS and signal propagation path, procedures on the selection of receiver's data using iteration method, relevant pseudocode algorithms for arriving localization solutions, and results are presented in Section 4. Finally, conclusions are discussed in Section 5.

Notation: $\forall$ denotes for all; $\in$ denotes an RSS belongs to a set; R denotes the location; $\hat{d}$ denotes the estimated model distance; $\vee$ denotes the compound statement of OR; $\downarrow$ Unicode represents the next instruction; $\cap$ denotes common intersection values.

2. THEORETICAL BACKGROUND

There are two important aspects of indoor localization. One is to find out an optimal path loss model, and the other one is to obtain the best trilateration approach to localize the source. In addition, optimal receiver module placement for localization is useful for achieving better accuracy. The geometrical changes in the placing of the modules always enlighten new types of problems and bring a new type of method for arriving at the solutions [8, 9]. For several reasons a better configuration of placing the sensor is important, notably, finding the trajectory path of the source, better energy saving with unused nodes, and also for repairing the network in dead nodes with neighboring nodes. Our earlier results indicate that by placing the modules at the vertices of an isosceles triangle will offer a wide separation between the modules resulting in improvement of the Dilution of Precision (DoP) [10].

Consider a typical corridor experiment scenario with an office environment as shown in Figure 1. Solid lines represent the real-time coverage area by the modules, and dashed circles represent the ideal coverage scenario. Estimation of source position is critical in the shaded regions. The present work concentrates on these shaded regions.

The indoor signal strength measurements play a critical role in both localization and 5G communication problems. Several researchers have reported their work on modeling aspects, and it is well established that the performance of communication channels is a function of environment, generation devices, different data rates, etc. [11–13]. [14] presented various wireless indoor positioning systems and their analyses in terms of accuracy, scalability, cost, precision, robustness, and complexity. Recently, [15] proposed a GNSS augmented Bluetooth Low Energy (BLE) based indoor localization system by data fusion of GNSS and BLE. By the careful use of low-power modes for GNSS, inertial sensing and the CC2640R2F blue tooth module with a Cortex M3 microcontroller, combined with a LoRa backhaul provide a power-efficient navigation solution in an indoor office environment.

[16] presented a 3D Indoor Localization Based on Wi-Fi and built-in-sensors (3D-WFBS) with
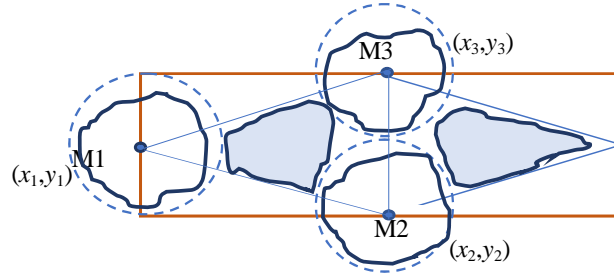
Figure 1. The receiver modules are at the vertices of an imaginary isosceles triangle of rectangular shape office corridor.

the help of Fine Time Measurement Protocol. From the pedestrian's real-time heading, walking speed, received signal strength indication, and round-trip time collected from Wi-Fi access points and combined for proximity detection sensors achieved 1 m level indoor localization accuracy. Similarly, [17] proposed RSS-based Indoor Passive localization using clustering and filtering in LTE networks. In all these experimental scenarios, the role of hardware modules is critical. To solve indoor localization and communication problems and to evaluate channel performance, a thorough investigation of measurement data is essential.

To model the performance of off-the-shelf hardware modules in the indoor environment, in our current work we considered the logarithmic (log-linear) regression model. It is mathematically expressed as
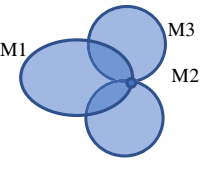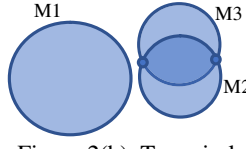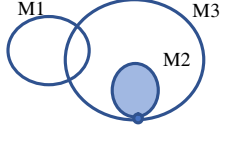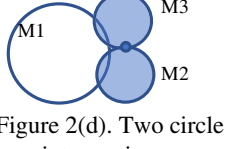
$$y = \beta_0 + \beta_1 * \ln(x)$$
$$\beta_1 = \frac{\sum \left(\ln x_i - \overline{\ln x} \right) \left(y_i - \bar{y} \right)}{\sum \left(\ln x_i - \overline{\ln x} \right)^2};$$
$$\beta_o = \bar{y} - \beta_1 \overline{\ln x}$$

(1)

where 'β_0' is the intercept and 'β_1' the slope of the regression line, and 'y' the measured signal strength at a distance of 'x' in meters. Logarithmic regression is a parabolic shape. The logarithmic regression model is chosen because it more closely emphasizes the RSS measurements for distance range. It is preferred because it fits well with measured data for a large variance [18]. The sensitivity of this model is examined by various authors with Root Mean Square Error (RMSE), and it is found that the results are stable and truly reflect in the localization result [19–21].

In the context of source localization for the indoor environment, there is no such good model available to suit multipath characteristics except using the traditional trilateration or proximity algorithms to mitigate the measurement errors [14]. The quality of the trilateration of circles is discussed by [22] in terms of uncertainty, nonconsistency, ambiguity, and error propagation. The reported work enables the researchers to observe the different geometric forms of trilateration circles and also helps in avoiding poor trilateration for source localization. Table 1 presents the list of problem formulation scenarios and their solutions relevant to our work [35].

For a given corridor, three-receiver modules M1, M2, and M3 are placed at the vertices (x_1, y_1), (x_2, y_2), and (x_3, y_3) of an imaginary isosceles triangle as shown in Figure 1. The signal strengths received at these three modules are RSS1, RSS2, and RSS3. The source is located at (x_s, y_s) on the median line of the corridor. The radii of the theoretical coverage area offered by the modules are estimated from the logarithmic regression model and are represented as r_1, r_2, and r_3 (Table 1). In the case of indoor RSS measurements, being random in nature multiple measurements are needed at each predefined position. Out of these measurements for the selection of optimum value, we have to follow the process of comparison with the modelled value. Whichever measured value is close to the modelled value is considered as the optimum value. Based on such optimum values for each predefined position, the entire corridor is divided into different segments. For each segment, a modified propagation path loss model is evolved. In each segment, different scenarios may exist which are shown in Table 1 and Figure 2.

Table 1. Various scenarios of trilateration method for source localization.

S No	Problem Formulation	Scenario	Mathematical Expressions	Eq. No.
1	Measured RSS1, RSS2 and RSS3 are nearly equal to modelled RSS.	Figure 2(a). Three circles exactly intersect.	$$A = \begin{pmatrix} 2(x_3 - x_1) & 2(y_3 - y_1) \\ . & . \\ 2(x_3 - x_2) & 2(y_3 - y_2) \end{pmatrix}$$ $$B = \begin{pmatrix} x_s \\ y_s \end{pmatrix}$$ $$C = \begin{pmatrix} r_1^2 - x_1^2 - y_1^2 - (r_3^2 - x_3^2 - y_3^2) \\ . \\ r_2^2 - x_2^2 - y_2^2 - (r_3^2 - x_3^2 - y_3^2) \end{pmatrix}$$ Based on the least square system, the estimated position is $$B = (A^T \cdot A)^{-1} \cdot A^T \cdot C$$	(2)
2	RSS2 and RSS3 are nearer to modelled values and causing flip ambiguity	Figure 2(b). Two circle intersection.	$$x_{s,2,3} = \frac{(x_2 + x_3)}{2} + \frac{(x_2 - x_3)(r_2^2 - r_3^2)}{2D^2} \pm \frac{2(y_2 - y_3)}{D^2} * K;$$ $$y_{s,2,3} = \frac{(y_2 + y_3)}{2} + \frac{(y_2 - y_3)(r_2^2 - r_3^2)}{2D^2} \mp \frac{2(x_2 - x_3)}{D^2} * K$$ *and constant k* $$= \frac{1}{4}\sqrt{(D + r_2 + r_3)(D + r_2 - r_3)(D - r_2 + r_3)(-D + r_2 + r_3)}$$ *distance between circles* $(D) = \sqrt{(x_2 - x_1)^2 + (y_2 - y_1)^2}$ *estimated source* $= (x_{s,2,3}, y_{s,2,3})$	(3)
3	Severe noisy measurements of M2 and M3 results in multipath.	Figure 2(c). One circle circumscribes another circle.	$$x_s = \frac{r_2(x_3 - x_2)}{(r_3 - r_2)} + x_2; \quad y_s = \frac{r_2(y_3 - y_2)}{(r_2 - r_3)} + y_2$$ The estimated source $= (x_s, y_s)$	(4)
4	For M2 and M3 signals coming from different directions without interference.	Figure 2(d). Two circle intersection.	$$x_s = \frac{r_2(x_3 - x_2)}{(r_3 + r_2)} + x_2; \quad y_s = \frac{r_2(y_3 - y_2)}{(r_2 + r_3)} + y_2$$ The estimated source $= (x_s, y_s)$	(5)

The four problem scenarios which we came across in our experimentation are summarized in the table. Scenario 1 represents the case when all the three measured RSS values are well fitted. In the second scenario, the RSS values of the two modules are similar whereas the RSS of the third one is such that its circle is not intersecting the other two circles. The intersection of circles at two points is due to flip ambiguity, and one of them is source position. Several localization solutions fall under this scenario because distributed localization is performed with a sparsely connected wireless network. The third scenario is an uncertainty situation realized from noisy ranging measurements in multipath conditions. In this case, potentially RSS values of two modules are interfering with each other either constructively or destructively. In such a case, all the three circles are not intersecting at the same point; also one circle circumscribes another circle; and approximate localization has arrived from the tangency point of the latter two circles. The fourth and the last scenario is very similar to the third scenario where multipath propagation conditions exist. Unlike the third scenario, no circle is circumscribing the other circle. For example, at the center of the corridor where the two modules are placed opposite to each other, a breakpoint occurs, and dual slope models are applied. Therefore, the condition for arriving at the localization solution is different from scenario three. In Table 1, to classify different localization

scenarios, the measured RSS (RSS_meas) values are compared with RSS values due to logarithmic regression model (RSS_model). The relevant mathematical expressions for localization solutions for all four scenarios are given in the table. The Summary of Reviewed works and Distinctive Characteristics along with present work are presented in Table 2.

2.1. Computational Complexity

In the proposed method, we considered three modules in an isosceles triangle shape to cover the rectangular office corridor. For a localization process, it is important to know how many receiver modules are essential. Generally, it is assumed that a large number of receiver modules lead to better localization solutions; however, this assumption is to be reconsidered as it leads to increased complexity. The complexity involved here is the selection of algorithms for an optimal number of modules to deal with this problem. The suggested dynamic circle expansion/contraction algorithms will help in solving this problem. Salient features of the computational complexity are summarised in Table 3.

3. EXPERIMENTAL SETUP

Experiments are conducted in the ground floor corridor (3.57×21 m) of the Research and Entrepreneurship (R & E) Hub of CBIT. The hub is a newly constructed two-year-old building with reinforced concrete and a polished stone corridor. Office rooms, a pantry, a large conference hall, and a mini-conference room are located on either side of the corridor. The doors of the rooms are made of steel and have glass windows. The flooring is with natural granite stone, and the sidewalls are embedded with polished marbles. The floor plan is as shown in Figure 3. The effect of granite stone surface roughness, the smooth surface of marble, and the electrical properties of the surrounding environment created interest in our work. Such type of environment creates strong reflections, multipath, and shadowing effects on the wave propagation. Besides, the corridor is similar to the rectangular waveguide, and the theory for wave propagation in waveguides motivated us to develop an optimum path loss model in the corridor for future generation 5G networks. From Figure 3, it is clear that the experiment location is a source of multipath for the considered operating frequencies.
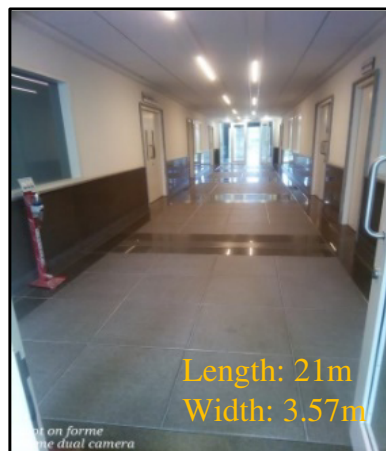

Figure 3. Floor plan of indoor corridor at R&E Hub, CBIT.

In such a scenario, knowledge of the effects of building materials and structures on wave propagation is essential. When such information is available, a system designer can do a thorough analysis of measurement data. Several experimental results on the attenuation of an electromagnetic wave in indoor corridors are reported by various authors [23–25]. Similarly, the electrical properties of interior construction material are discussed by [3, 26–29]. [30] summarized the electrical properties of various materials.

Table 2. Summary of reviewed works and distinctive characteristics along with present work.

S No	Author	Related Work	Distinctive Characteristics	Conclusions of work
1	Hema Achanta et al., [8, 9]	Optimum Sensor Placement of Receiver Modules in the 3D scenario.	The source is uniformly distributed in a sphere and sensors are placed outside a larger concentric sphere. The Fisher Information matrix is used for optimizing the source position by maximizing the smallest eigenvalue.	Simulation results showed that optimum sensor placement has a better performance compared to arbitrary sensor placement.
2	Robert J. C. Bultitude [11]	Reported Continuous wave propagation experiments at 910 MHz in an indoor environment.	Reported statistics such as power and phase variations concerning time. CDF for CW fading signal is presented for indoor environment.	The received power varies at $R^{-1.8}$, where R represents the distance and diffraction losses (10 to 15 dB).
3	A. D. Sarma [12]	Reported propagation experimental results at 60 GHz.	Ott and Thompson's model is used to discuss the significance of the refractive index. Practical aspects of models are explained.	Meteorological conditions play an important role in oxygen absorption at 60 GHz frequencies.
4	T. S. Rappaport [13]	Reported multipath propagation measurements at 1300 MHz.	Multipath spread, mean excess delay, RMS Delay Spread, and magnitude of Transfer function multipath are observed.	Estimated path loss is highly correlated with distance. Average values of all multipath channel parameters are presented.
5	Liu et al., [14]	Provided an overview of the existing wireless indoor positioning systems, techniques, and solutions.	Typical Location estimation schemes are analyzed. Fingerprinting technique is discussed in detail.	Different performance measurement systems are evaluated and discussed at length.
6	Dai et al., [15]	Proposed GNSS augmented Bluetooth Low Energy (BLE) based indoor localization system by data fusion of GNSS and BLE.	Developed hardware with a microcontroller, GNSS module, Bluetooth module, active Bluetooth beacons, LoRa, and MEMS sensors and performed real-time experimentation.	The proposed method achieved better than 4 ms accuracy in an indoor office environment.
7	Y. Yu et al., [16]	Proposed a hybrid localization technique using Wi-Fi finite time measurements and smartphone in-built sensors.	Used adaptive extended Kalman filter algorithm for estimating pedestrians' real-time heading, and walking speed. Combining with Wi-Fi Access points estimated the range.	With the proposed algorithm '3D-WFBS' a meter level accuracy in a typical indoor environment is achieved.
8	Zheng et al., [17]	Proposed an LTE network environment for indoor localization.	WKNN is used for classifying the regions and obtaining localization results which are compared with the LTE network environment.	Proved that the proposed LTE network environment gives 24% better accuracy than the WKNN method.
9	T. Sridher et al., (proposed work)	Presented hybrid source localization technique.	Optimum path loss models are derived. Corridor segmentation is done. Concentrated on performance degraded parameters to improve the localization accuracy.	Achieved better segment-wise standard deviation errors in x and y directions.

Table 3. Computational complexity in hybrid localization.

Problem Formulation	Mathematical Expression	Complexity
Model formation with Noisy Ranging measurements in Extended Corridor environment	$RMSE_{mes(p)} = \sqrt{\frac{\sum_{q=1}^{n}(RSS_{model\,p,q}-RSS_{mes\,p,q})^2}{n}}$	Poor range measurements due to isosceles triangle shape and multipath environment are avoided by analyzing RMSE values of modules 2 and 3.
Selection of optimum RSS value	$RSS = \text{find}\{\min(d_i), \text{ measured RSS}\}$	The least-square estimation method finds the distance error and later on uses the bubble sort algorithm for finding the nearest value to the model.
Grouping segments	$RMSE_{M1,M2,M3} =$ $\begin{cases} RMSE_{M1}<RMSE_{M2,M3} \vee RMSE_{M1,M2,M3} \downarrow \\ RMSE_{M1}>RMSE_{M2,M3} \vee RMSE_{M1,M2,M3} \uparrow \end{cases}$	The iterative procedure selects the minimum RMSE value in the segments. The selection of RMSE depends upon the evolved new model.
Flip Ambiguity	Localization Solution arrived from Eq. (3). Where r_2, r_3 are replaced with r'_2, r'_3 $r'_{2,3} = r_{2,3} - \left(\frac{r_1}{2}\right)$ $RSS_{M2,M3} > RSS_{threshould}$ $r'_{2,3} = r_{2,3} + \left(\frac{r_1}{2}\right)$ $RSS_{M2,M3} < RSS_{threshould}$	The mirror image of the results confuses the localization. The solution can be arrived with dynamic circle expansion.
One circle circumscribes another circle due to Severe noisy measurements of M2 and M3 resulting in a multipath.	Localization Solution arrived from Eq. (4). Where r_2, r_3 are replaced with r'_2, r'_3 $r'_{2,3} = r_{2,3} - \left(\frac{r_1}{2}\right)$ $RSS_{M2,M3} > RSS_{threshould}$ $r'_{2,3} = r_{2,3} + \left(\frac{r_1}{2}\right)$ $RSS_{M2,M3} < RSS_{threshould}$	Failure in trilateration is overcome by the presented technique.

The ceiling of the corridor is made up of white Plaster of Paris (POP) gypsum boards supported with pendant linear LED lights along the roof of the corridor. POP is supported by metal studs made of steel. During the experiment, the doors of all the rooms closed to facilitate a line-of-sight environment also. By examining the electrical characteristics of the corridor environment, it is obvious that the attenuation levels experienced by the propagating waves are different for different materials.

Five Wi-Fi transceiver modules (ESP 8266), micro USB cables, and a laptop (4 GB RAM) for data logs are used in the experiments. The supply voltages for the modules range from 2.5 to 3.6 V. The modules operate in the frequency range of 2412–2484 MHz. The typical operating frequency is 2400 MHz [36]. Modules have an in-built 8-bit microcontroller. Two types of codes are run on this microcontroller. The first one is the application code, where the signal strength measurement code has been written in it. The latter one is the firmware. It is a low-level code that supports the application code. The current consumption is between 15 μA and 400 mA. Wi-Fi is included in these transceivers.

During the experiment, these modules are programmed to work as both transmitter and receiver. These modules are powered by an external power supply. Modules user id (Service Set Identifier:

SSID) is visible to the Wi-Fi operated devices. Modules are placed at the vertices of an isosceles triangle (A, B, and C) with an adjacent side length of 10.6 m as shown in Figure 1 to achieve a better Dilution of Precision (DoP) in source localization. The adjacent channel reduction ratio 31 dB makes the interference insignificant. The transmitter and receiver modules are placed at a height of 75 cm from ground level to avoid the ground reflections. A program is developed to estimate the received signal strength and is installed in the receiver modules. Experiments are conducted for source localization based on the signals received from the fixed receivers. The results of these experiments are intended for examining the efficiency and scalability of the proposed localization approach and for developing a prototype system for source localization in the office environment. The measurement system consists of receivers in predefined locations while the source was moved along the centerline of the corridor. The RSS at each of the three-receiver modules is recorded for each source position along the center line of the corridor for every 0.25 m. The sampling period of RSS measurements is 1 sec. These experiments are conducted in the daytime on weekdays, with personnel moving throughout the corridor. Therefore, there is a minor influence of the shadowing effect and pedestrian traffic on the measurements.

In our experiment, as the source moves towards the other end of the corridor, the localization solution is not satisfactory due to huge multipath interference from the surroundings. Therefore, we placed another receiver module M4 at location D, exactly opposite to module M1 and at a distance of 22 m. By considering the RSS values from modules M2, M3 and M4, better localization accuracy is achieved.

4. RESULTS AND DISCUSSION

In this section, initially, we examined the relation between Received Signal Strength (RSS) and propagation path distance using the logarithmic regression model. Later on, we investigated the selection of receivers data from the high signal strength measurements for indoor localization using the iterative method and subsequently estimated the source position using the trilateration principle.

4.1. Examining the RSS and Propagation Path Distance

In our early work, we employed a straightforward linear regression method to estimate the distance between the source and the receiver [10]. However, this model provides a poor localization solution leading to large positional errors. The reasons are examined in the present work. One of the reasons is that in the trilateration method, the three circles are not intersecting at a common point. This is the most common uncertainty in trilateration under noisy ranging measurements, especially in an indoor environment. The second reason is that the measured data trend is following a cone shape on the plot between the model and measured data indicating that the error due to the model does not have constant variance [34]. The presence of non-constant variance suggests that there are some unusual RSS samples in the data which must be studied closely to make a better model.

So, in this work, we focused on improving the localization accuracy by choosing an appropriate ranging estimation model. To address this aspect, we worked on establishing a relation between the RSS and propagation path distance using the logarithmic regression model. In our examination, to model the propagation path of the wave under an indoor environment the logarithmic regression model is preferred for the following reasons: the first one is propagating radio wave's wavefront divergence. Wavefront divergence is the edge of the propagating wave. As the wavefront propagates spherically, its surface enlarges; consequently, its power density decreases with the square of the distance [30]. The indoor environment makes the propagating wave to fluctuate due to multipath and attenuation, causing the RSS to be nonlinear. The point where the signal strength fluctuates with different slopes is called the breakpoint. The region after the breakpoint is similar to the behavior of the logarithmic curve at a decibels distance, unlike the linear curve. A large number of path loss models are represented in terms of dual slopes for the cases of the corridors and tunnels [31]. The second reason for preferring the logarithmic regression model is that the logarithmic expressions are a more convenient means of transforming a highly skewed variable into one that is more approximately normal. Due to these reasons, we preferred logarithmic regression in this current work.

The direct path distances from the source to receiver modules are considered as 'd_1', 'd_2, and 'd_3'
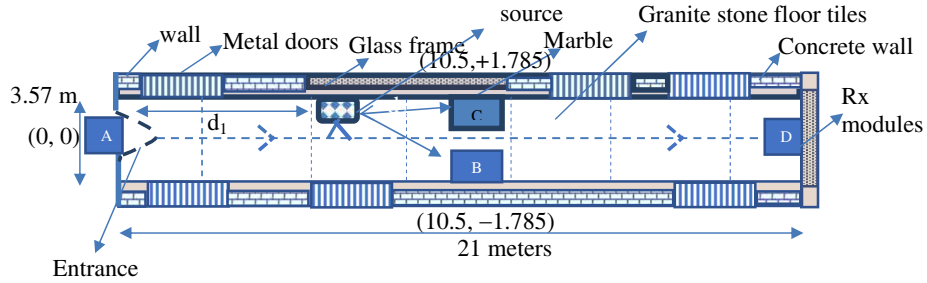
Figure 4. Experiment scenario at R&E Hub, CBIT.

(Figure 4). The source positions along the centerline of the corridor are represented as $S_1, S_2, S_3, \ldots, S_{21}$. The estimated logarithmic regression models for M1, M2, & M3 in the corridor can be expressed respectively as:

$$y_1 = -57.90 - 5.25 * \ln(d_1) \quad 1 < d_1 < 21 \tag{6}$$

$$y_2 = -45.73 - 5.566 * \ln(d_2) \quad 1.8537 < d_2 < 10.6506 \tag{7}$$

$$y_3 = -54.6 - 3.669 * \ln(d3) \quad 1.8537 < d_3 < 10.6506 \tag{8}$$

where 'yi' is a modelled RSS value at a distance of d_1, d_2, and d_3. Corresponding regression plots for measured data are shown in Figure 5.
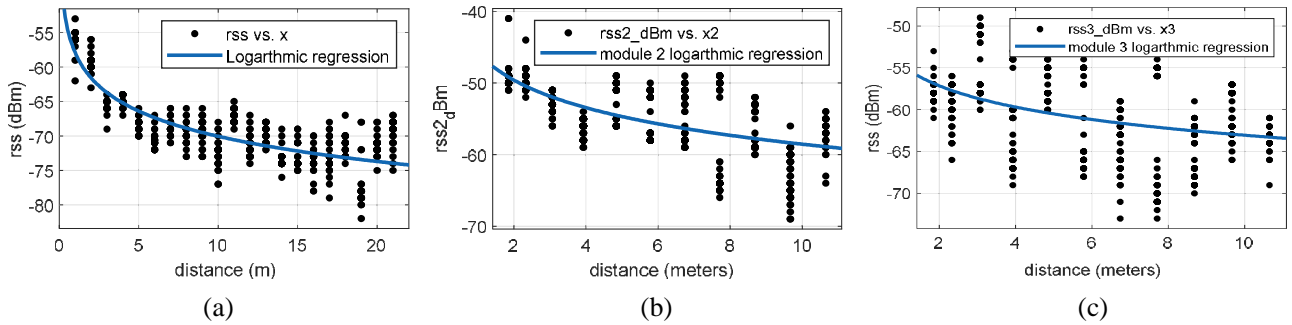

Figure 5. (a) M1 logarithmic regression curve. (b) M2 logarithmic regression curve. (c) M3 logarithmic regression curve.

The RSS values along the corridor assume a parabolic shape (Figure 5). The plots show the behavior of homoskedasticity [32]. In most of the locations, RSS values follow the models. It implies that the errors are normally distributed. Also, from Figure 5, we can observe that at very few locations the RSS values are deviating from the models. This results in a non-constant variance in the error at these locations. This can be observed in the RMSE plot at the corresponding locations (Figure 6). These locations are influencing the models and subsequently the performance of localization. Apart from estimating the RMSE, the quality of obtained models (Eqs. (6), (7), and (8)) are examined with statistical parameters namely Correlation Coefficient (R^2) and Adjusted R^2 (Table 4).

Table 4. Performance parameters for modules data.

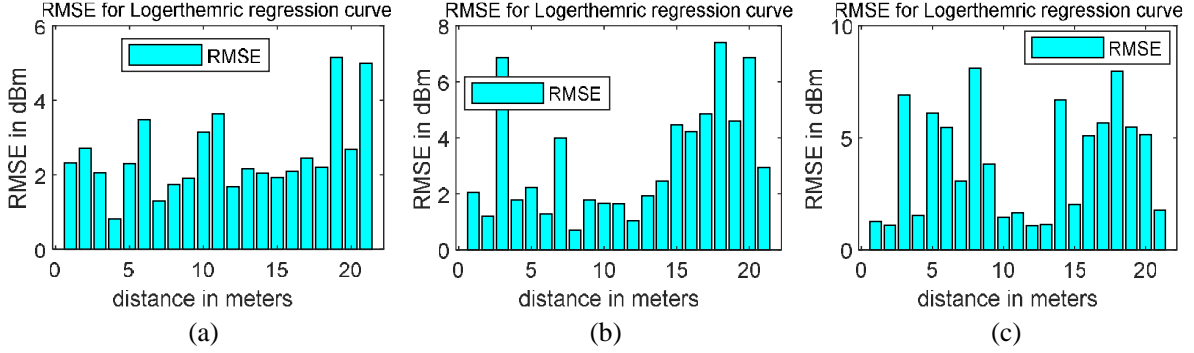| S No	Module	R^2	Adjusted R^2
1	M1	70.47%	70.43%
2	M2	40.4%	40.3%
3	M3	16.09%	15.96%

Figure 6. (a) RMSE for M1 data. (b) RMSE for M2 data. (c) RMSE for M3 data.
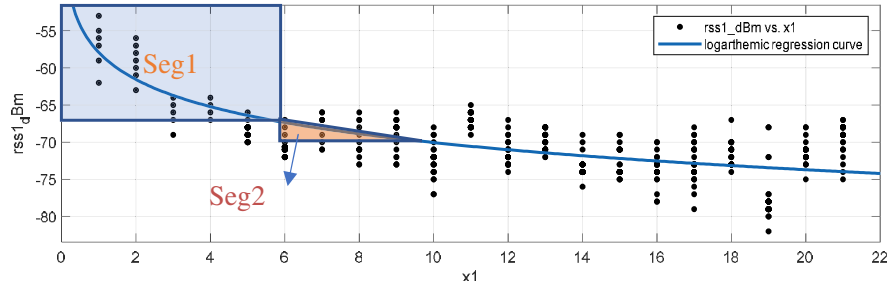

Figure 7. Division of M1 data segments in the corridor.

RMSE values due to the three modules M1, M2, and M3 are shown in Figure 6. The higher RMSE values could be due to the influence of corridor materials, multipath, measurement error, antenna positioning, etc., R^2 shows how best the data fit the model. The chances of improving the model by introducing a new parameter are represented by adjusted R^2. These two parameters for M1 are above 50%, and in the other two cases, they are far less than 50%. These values clearly show the necessity of improving model accuracy. Therefore, to improve the performance of the models, the corridor is divided into 2 segments. For each segment of data, a new appropriate model is framed to best fit the experimental data (Figure 7).

Initially, regression models are developed for 0–6 m of the corridor for all three modules. In this range, the RMSE values are higher for all modules. From Figure 7, we can notice that the signal strength values greater than -67 dBm are considered as the first segment. We can also observe in the figure that even after the S_6 location the measured values are better than -67 dBm. But these are far away from the model. To optimize source position, a valid RSS measurement that is close to the model is considered in our experiment. For that measurement, only the relevant model is applied. The new regression models for the first segment are expressed as:

$$y_1 = -55.2435 - 8.1058 * \ln(d1) \quad 1 < d_1 < 6 \tag{9}$$

$$y_2 = -45.4349 - 6.9688 * \ln(d_2) \quad 4.8411 < d_2 < 9.6662 \tag{10}$$

$$y_3 = -36.61 - 11.26 * \ln(d_3) \quad 4.8411 < d_3 < 9.6662 \tag{11}$$

A similar procedure is followed to examine these new regression models with the help of RMSE, R^2, and adjusted R^2 values (Table 5).

It is obvious from Figures 8(a) and 6(a) that in the range of 1–6 meters the RMSE values are improved due to the new model. However, at the location of S_3, the RMSE is large for both M2 and M3. Therefore, we can expect a large error while performing the source localization at this location. The reasons for the large error at location 3 are examined based on Figures 5(a) & 5(b) results.

Figure 9 compares the measurements with the improved model (Eqs. (10) and (11)). When the source is at location S_3, and M2 and M3 measured data are far away from the new model. It indicates

Table 5. The performance parameters of new model data.

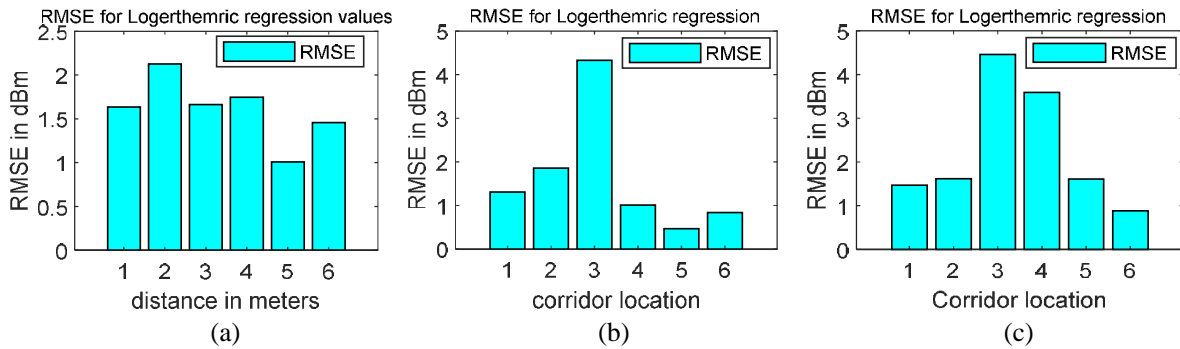| S No	Module	R^2	Adjusted R^2
1	M1	89.93%	89.87%
2	M2	38.44%	38.1%
3	M3	50.88%	50.8%

Figure 8. (a) M1 RMSE estimation using model y_1. (b) M2 RMSE estimation using model y_2. (c) M3 RMSE estimation using model y_3.
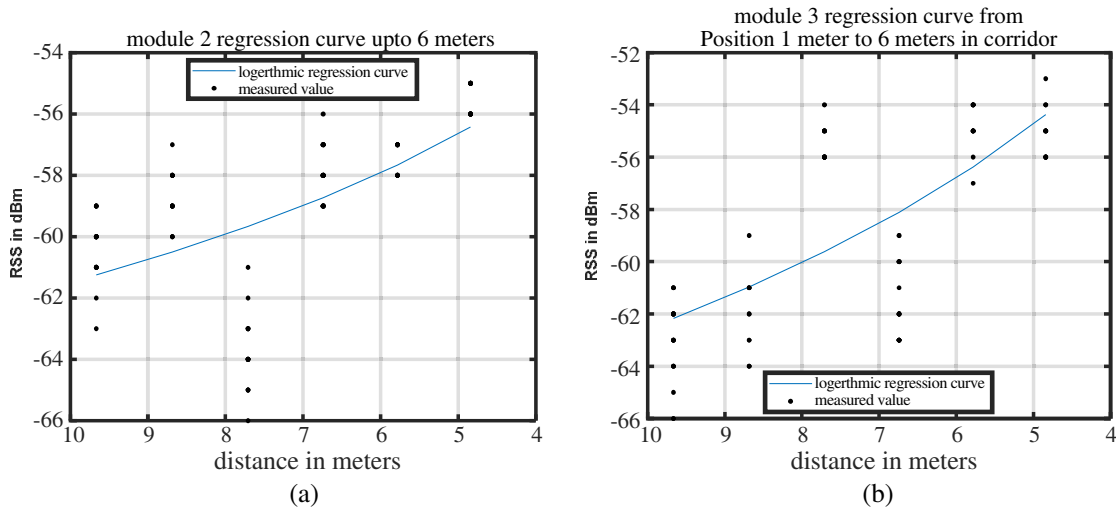

Figure 9. (a) Module 2 new regression model. (b) Module 3 new regression model.

that the measured RSS values are severely affected by surrounding environment noise. This S_3 location in the corridor is falling in scenario 3 of Table 1. For all other locations in the corridor of the 1–6 meter range, the RMSE is very low (Figures 8(b) and 8(c)). Therefore, the localization comes in the scenario of either 1 or 2 (Table 1).

Similarly, analysis is carried out for the second segment. In the second segment, a 6–11 meters corridor range is considered (highlighted with red color in Figure 7). Before evolving the new model in these locations, the previous models (Eqs. (9), (10) & (11)) are examined. If these models perform well with these measured data, then these models can be extended to these locations. Otherwise, a new model is necessary. A similar analysis is followed for the remaining locations up to 21 m in the corridor. For example, the extended model and corresponding RMSE for M1 in the locations of S_1 to S_{11} are shown in Figure 10.
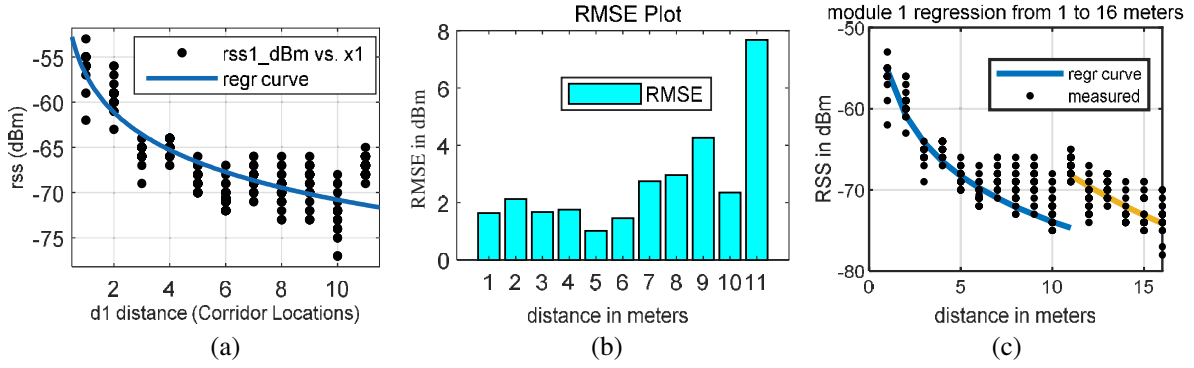
Figure 10. (a) regression curve upto 11 meters. (b) RMSE upto 11 meters. (c) Regression curve upto 16 meters.

The model performs well up to S_{10} location (RMSE ≤ 4). However, at the S_{11} location, the model does not satisfy the measurement data, and the same is reflected in the RMSE plot (Figure 10(b)). At the S_{11} location, the propagating signal experiences large path loss and fluctuations due to the nearby environment where M2 and M3 are located. Therefore, this model is not suitable at this location (S_{11} location) and is called a breakpoint. It has arrived from the analysis of measurement data in Figure 10(c), which is close to the breakpoint distance arrived from Eq. (12) of [23].

$$d_{break} = \sqrt{\frac{a}{\lambda}} \, meters \tag{12}$$

where a is the maximum dimension of the corridor (21 m), and 'λ' is the wavelength of the propagating wave. The breakpoint arrives at 13 meters. The localization solution for S_{11} comes under scenario 2 (Table 1).

In our experiment, the idea of framing the segments in the corridor is for the improvement of the localization accuracy with the proposed model. When the source is moved along the center of the corridor, each receiver module collects the signal strength and SSID information. Later on, this information is transferred to the post-processing unit for further localization purposes. The receiver modules are placed in different locations in the corridor. The environment around the modules is different for different modules, so the effects are different necessitating a unique model for each module.

As M1 is on the centerline of the beginning of the corridor, estimating the propagation path distance from the source is straightforward (Eq. (13)).

For M1:

$$d_1 = \begin{cases} e^{\frac{-(RSS+55.243)}{8.1058}}, & RSS \geq -70 \, \text{dBm} \\ e^{\frac{-(RSS+30.287)}{15.189}}, & RSS < -70 \, \text{dBm} \end{cases} \tag{13}$$

However, model equations for M2 and M3 are different as they are positioned on either side of the centerline. The region among M1, M2, and M3 is considered the first segment. The rest of the region is the 2nd segment.

To know in which segment the source lies M1 data modelling is necessary. Once it is known the modelling of M2 and M3 data can be done. If the source is in the first segment, then the signal received by M1 is stronger than the signal received from the source in the second segment (Figure 11). A similar analysis for M2, M3 is discussed by [33] for identifying the source position using the geometry of a half plane-symmetric lens. Based on these concepts, the proposed models for estimating the distance for M2 and M3 are expressed as:

For M2:

$$d_2 = \begin{cases} e^{\frac{-(RSS+45.43)}{6.97}}, & \forall RSS \ \ for \ segment \ A \\ e^{\frac{-(RSS+49.1)}{2.09}}, & \forall RSS \ \ for \ segement \ B \end{cases} \tag{14}$$
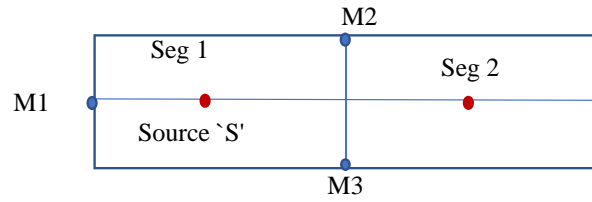
Figure 11. Representation of source position in the corridor as a half symmetric planes.
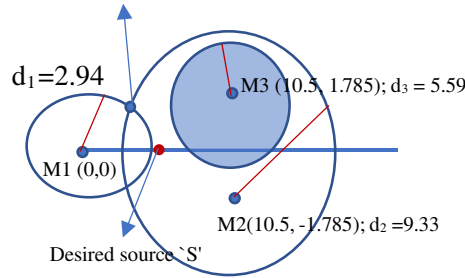

Figure 12. Localization at source S_3 position.

For M3:

$$d_3 = \begin{cases} e^{\frac{-(36.614+RSS)}{11.2648}}, & \forall RSS \;\; for\; segment\; A \\ e^{\frac{-(53.3109+RSS)}{6.1075}}, & \forall RSS \;\; for\; segment\; B \end{cases} \tag{15}$$

4.2. Source Localization

Once RSS-based distance estimation is done successfully, the next step is source localization. We used a circle-based geometric trilateration algorithm. For various localization scenarios, we developed tiny pseudo-code algorithms (Table 1). These algorithms help in the decision process for obtaining better accuracy. The advantage of these algorithms is its simplicity in implementation and easy to analyze the problems in localization. The source can be localized based on the intersection of the coverage area circles of M1, M2, and M3 modules. Each coverage area is due to respective modeled data. The larger the coverage area is, the more the localization error is. The source becomes non-localizable if it does not lie within the coverage area of any two circles. In our work, we consider the source movement one dimensional; therefore, the intersection of any two overlapping circles gives the localization. As the source moves from Module 1 to the bisector point M2–M3, the signal strength at M1 decreases whereas at M2, M3 strength improves. Therefore, M2 and M3 coverage area is used for localization purposes. When the source moves towards the other end of the corridor, the RSS of all the modules decreases necessitating new models which consider environmental losses.

Initially, the signal strength information received by M1 is used for dividing the corridor into segments for developing individual model equations. Then with the help of information from M2 and M3 along with the M1 model the source position is estimated.

During this stage, data profiling, data cleaning, and removing outliers are performed with customized methods. For selecting the optimum RSS value w.r.t the developed model a pseudo-code algorithm is developed (Algorithm 1). The same procedure is implemented for both segments.

Similarly, the pseudo-code for identifying the segment based on hierarchical segmentation from top to down order is given in Algorithm 2. We assigned a threshold to these segments and observed the behavior of measured RSS in the corridor environment in the context of segmentation. Initially, two independent models 1–6 m and 6–11 m are developed. Based on the correlation coefficient between these models, the two are combined to one effective model. The pseudo-code for combining the clusters is shown in Algorithm 3.

Algorithm 1 Pseudo code for selection of RSS.

Input: Measured RSS value, True distance
Output: Nearest RSS value
1: $\text{RSS}_i \in \mathcal{R}$/Measured Data at each location $\{\text{RSS}_1, \text{RSS}_2, \ldots, \text{RSS}_{30}\}$
2: d_i/Original distance
3: **for** each measured RSS value **do**
4: Calculate Eq. (8)/obtain model distance
5: $d_i = |d_i - \hat{d}|$/Difference between original and model distance
6: RSS = find $\{\min(d_i),$ measured RSS$\}$/find minimum difference and concern RSS value
7: **end**/store the nearest RSS value

In our study, the experiment environment consists of four types of scenarios (Table 1). The intersection of circles will evaluate the source position. It depends upon the selection of any two circles, because of the 2-D environment.

Algorithm 2 Pseudo code for identifying segments.

Input: Measured RSS samples
Output: Estimated distance of all three modules
1: $\text{RSS}_{Mi} \in \mathcal{R}$/Data at each location from all three modules $\{\text{RSS}_1, \text{RSS}_2, \ldots, \text{RSS}_{30}\}$
2: **Identify** the M1, M2, and M3 data using SSID information
3: **Apply** logarithmic regression for M1 data for throughout the corridor
3: **Calculate** Correlation Coefficient R^2
4: **for** every measurement at each ith measurement location
5: **do** RMSE
6: if $\text{RMSE}_{M1} >$ defined error **then** \ at each measured location for M1
7: **define** segment with $\text{RSS}_{threshould}$
8: **do** thenearest **RSS** sample selection algorithm
9: **Repeat** the steps from 3 to 8 for M2, M3
10: **if** $RMSE_{M1,M2,M3} = \begin{cases} RMSE_{M1} < RMSE_{M2,M3} \ \vee \ RMSE_{M1,M2,M3} \ \downarrow \\ RMSE_{M1} > RMSE_{M2,M3} \ \vee \ RMSE_{M1,M2,M3} \ \uparrow \end{cases}$ **then**
11: segment is 'well behaved'
12: **for** each 'well behaved' segment **do**
13: trilateration
14: **end**

Algorithm 3 Pseudo code for combing the segments.

Input: Measured RSS value, True distance
Output: clustered data
1: $\text{RSS}_i \in \mathcal{R}$/Measured Data at each location $\{\text{RSS}_1, \text{RSS}_2, \ldots, \text{RSS}_{30}\}$
2: d_i/Original distance
3: **for** $i = 1$ to n/number of locations
4: $\text{Seg}_i = \{\text{RSS}_i > \text{RSS}_{threshould}\}$/above threshold RSS are considered as segment
5: **end for**
6: $\text{Seg}_i = \{\text{Seg}_1, \text{Seg}_2, \ldots, \text{Seg}_n\}$
7: **while** size $(\text{Seg}_i) > 1$ do
8: $(\text{Seg}_1, \text{Seg}_2) = $ minimum $R^2(\text{Seg}_1, \text{Seg}_2)$
9: remove $\text{Seg}_1, \text{Seg}_2$ from existing Seg_i
10: add $\{\text{Seg}_1, \text{Seg}_2)$ as new segment
11: $\text{Seg}_i = \text{Seg}_i + 1$
12: **end while**

Table 6. Localization comparison between three modules to selective two modules.

S No	True Source Position	Least Square principle with all three modules	Selection of modules in arriving localization
1	(1, 0)	(1.21, −0.49)	Not Applicable
2	(2, 0)	(2.23, −1.47)	(2.02, −0.23)
3.	(3, 0)	(2.99, 7.82)	(2.02, 2.13)
4.	(4, 0)	(3.64, −0.58)	(3.76, 0.14)
5.	(5, 0)	(4.89, 0.78)	(4.88, 0.33)
6.	(6, 0)	(6.20, −0.16)	Not Applicable

Initially, we followed two estimation procedures for source localization. In the first procedure, straightforward localization is estimated using the trilateration procedure, whereas in the second procedure we estimated the source position using the selected module's data based on the scenarios (Table 6). In this way, better position accuracy is achieved. However, at a few locations, the localization error is large. For example, at source position 'S_3' the localization error is large in both the procedures. The distances estimated using developed models and their localization scenario is shown in Figure 12.

It is similar to localization scenario 3, and one circle circumscribes the other. The M3 coverage is very small. It is due to constructive interference of the signals at receiver M3 leading to ranging errors at this location. The red color dot represents the expected source position. In most cases, circles do not intersect at a common point. Recently, several authors have addressed this type of problems [7, 6, 22]. In our work, we have concentrated on the analysis of data. Both strong signal at M3 and improper intersection of M1, M2 are the main reasons for the wrong position estimation. The possible solution for improving accuracy is to go for a 'circle contraction' method. The method is similar to the work proposed by [6] for addressing the noisy ranging measurements in indoor environments. In their work, the coverage area of circles is expanded until the circles intersect each other. However, in our method, at this location, we followed circle contraction for M2 and M3 data. The radius of the circle after contraction/expansion (d') is given as,

$$d'_{2,3} = d_{2,3} - \left(\frac{d_1}{2}\right) \quad RSS_{M2,M3} > RSS_{threshould} \tag{16}$$

$$d'_{2,3} = d_{2,3} + \left(\frac{d_1}{2}\right) \quad RSS_{M2,M3} < RSS_{threshould} \tag{17}$$

In Eqs. (16) & (17) the subtraction or addition denotes the circle contraction or expansion depends on the deviation of RSS from the threshold model values. The threshold values of RSS are considered as limits for avoiding over contraction or expansion. In both these equations, the RSS value of 'd_1' is considered as the reference distance. Using Eq. (16) the source localization at 'S_3' arrives as (2.927, 0.323) and compares well with the true value.

In Figure 13 the dashed circles represent the contracted circles corresponding to M2 and M3 modules. The intersection of M1, M2 gives the localization of the source as (2.92, 0.32); (2.65, −1.27). Due to flip ambiguity, the solution has two solutions. The pseudo-code for implementing the circle expansion or contraction is shown in Algorithm 4.

Toward the end of the corridor, in our experiment, we have come across a scenario where no circle is intersecting with the other. This type of problem is solved by modeling the data with empirical models. For this, we analyzed the measured data at those locations. The abnormal data is rectified by incorporating the particular environment loss into the model equation. The attenuation rate due to drywall is calculated as (ITUR 2015)

$$A = 1636\frac{\sigma}{\epsilon_r} \tag{18}$$

where 'σ' denotes the conductivity (S/m), and 'ε_r' denotes the relative permittivity (F/m). These two
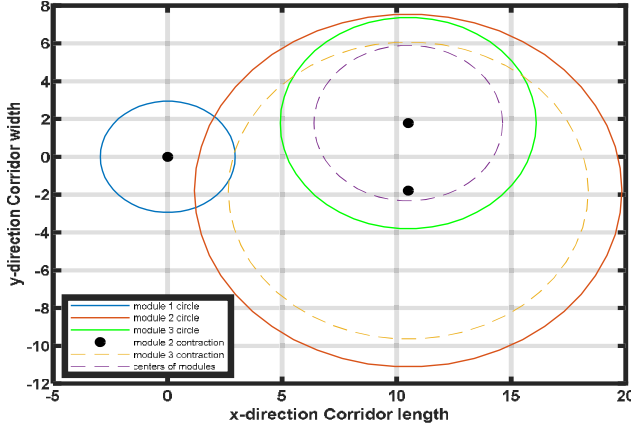
Figure 13. Localization of S3 using the circle contraction method.
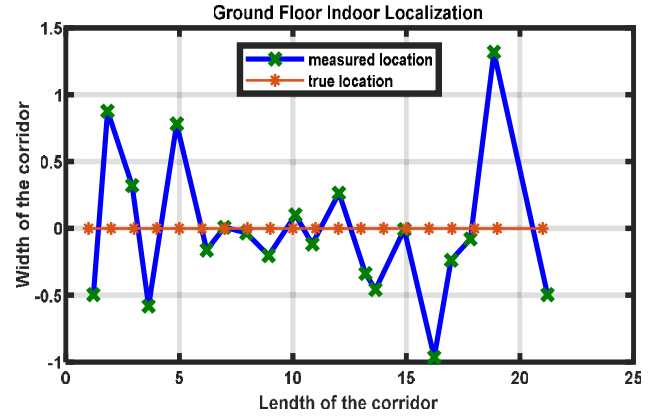

Figure 14. Localization of source in the R & E floor corridor.

Algorithm 4 Pseudo code for circle expansion/contraction.

Input: Measured RSS value
Output: Source Position
    Start

      1. C1, C2, C3 are circles drawn from the three receivers

      2. **Check** C1 ∩ C2 ∩ C3

      3. **If yes**

      4.   **Peform** trilateration

      5. **If not**

      6.   **If** C1∩ C2 then **do**

      7.   two circle intersection

      8.   **Else check** Contract/Expand C2 by a suitablemodel

      9.   **Return** step 6 and 7

      10.   **Else exit**

      11. **Perform** C1 ∩ C3

      12.   **Retrun** step 6 and 7

      13. **Else**

      14. **Perform C2 ∩ C3**

      15.   **Return** step 6 and 7

      16. **Else**

      17. Circle expansion failed **then** do

      18. Analyze the measured data

      19. Repeat from step 1

End

---

parameters are the functions of frequency. At $2.4\,\text{GHz}$ the values for drywall are $20\,\text{dB/m}$. According to the wave propagation environment, the attenuation rate is considered as positive or negative. The modified model equations at these locations are represented as the

$$y = \beta_0 + \beta_1 * \ln(x) + \gamma \tag{19}$$

where 'γ' represents the wall correction factor used as the constant to improve the model equation in

the segments. The improved model equations are used at 'S_{20}' where the $\mathrm{RSS}_{M1,M2,M3}$ much deviate from the models. The localization at 'S_{21}' is solved by placing the fourth receiver module at 22 meters from the corridor, and the source position is estimated at S_{21} location.

From the above analysis, the arrived localization in the corridor in all 21 locations is shown in Figure 14. Except at very few locations in segment two, the remaining locations' localization in the corridor is satisfactory. The standard deviation values of localization are summarized in Table 7.

Table 7. Segment wise localization errors.

Segment	Coordinates	Standard Deviation
First segment	X	$0.16\,\mathrm{m}$
(1–11 locations)	Y	$0.46\,\mathrm{m}$
Second Segment	X	$0.19\,\mathrm{m}$
(11–21 locations)	Y	$0.61\,\mathrm{m}$

The presented results in terms of accuracy may not compete with the results due to the latest localization devices, but our proposed method with low cost hardware is still better and useful for some of the localization applications like in indoor shopping malls, vehicle tracking, and localization of goods in industries.

5. CONCLUSIONS

Localization plays a vital role for Internet-of-Things and 5G communications. This paper presents a new indoor localization technique based on logarithmic regression model and circle expansion/contraction methods. The experiments are performed with off-the-shelf hardware modules which operate at $2.4\,\mathrm{GHz}$. We characterized the corridor into segments based on RSS values to improve localization accuracy. Accordingly, new model equations are framed in the segments. We presented the pseudo-codes for performing the segmentation. The localization scenarios faced in the given environment with suitable conditions are addressed, and the relevant numerical computations are given. The significance of the optimum placement of modules at the vertices of an isosceles triangle for better localization is also presented which facilitates easy implementation of circle contraction or expansion methods. The dynamic selection of modules improved the localization accuracy in x and y directions. Also, the hybrid computational techniques improved the localization accuracy in the cases of non-intersection of circles. These results and analysis could be useful for developing the future generation 5G networks in indoor office corridor environments. Adoption of the presented hybrid source localization method in the extended indoor corridor region where most of the data experiences a noisy environment may be further improved by techniques such as machine learning. The usefulness of the proposed mechanism in flip ambiguity which occurs in sparsely connected networks can be investigated. Further, the proposed work can also be extended to grid-based localization in residence areas.

REFERENCES

1. Omer, M., Y. Ran, and G. Y. Tian, "Indoor localization systems for passive UHF RFID tag based on RSSI radio map database," *Progress In Electromagnetics Research M*, Vol. 77, 51–60, 2019.

2. Mitilineos, S., D. M. Kyriazanos, O. E. Segou, J. N. Goufas, and S. Thomopoulos, "Indoor localisation with wireless sensor networks," *Progress In Electromagnetics Research*, Vol. 109, 441–474, 2010.

3. Obeidat, H. A., et al., "An indoor path loss prediction model using wall correction factors for wireless local area network and 5G indoor networks," *Radio Science*, Vol. 53, No. 4, 544–564, Apr. 2018, doi: 10.1002/2018RS006536.

4. Ciuonzo, D., P. S. Rossi, and P. K. Varshney, "Distributed detection in wireless sensor networks under multiplicative fading via generalized score tests," *IEEE Internet of Things Journal*, Vol. 8, No. 11, 9059–9071, Jun. 1, 2021, doi: 10.1109/JIOT.2021.3056325.

5. Ciuonzo, D., P. S. Rossi, and P. Willett, "Generalized rao test for decentralized detection of an uncooperative target," *IEEE Signal Processing Letters*, Vol. 24, No. 5, 678–682, May 2017, doi: 10.1109/LSP.2017.2686377.

6. Jiang, J., et al., "A distributed RSS-based localization using a dynamic circle expanding mechanism," *IEEE Sensors Journal*, Vol. 13, No. 10, 3754–3766, Oct. 2013, doi: 10.1109/JSEN.2013.2258905.

7. Wang, Z., H. Zhang, T. Lu, and T. A. Gulliver, "A grid-based localization algorithm for wireless sensor networks using connectivity and RSS rank," *IEEE Access*, Vol. 6, 8426–8439, 2018, doi: 10.1109/ACCESS.2018.2804381.

8. Achanta, H. K., S. Dasgupta, R. Mudumbai, W. Xu, and Z. Ding, "Optimum sensor placement for localization of a hazardous source under log normal shadowing," *Numerical Algebra, Control & Optimization*, Vol. 9, No. 3, 361–382, 2019, doi: 10.3934/naco.2019024.

9. Achanta, H. K., S. Dasgupta, and Z. Ding, "Optimum sensor placement for localization in three dimensional under log normal shadowing," *Proceedings of the International Congress on Image and Signal Processing (CISP)*, 1898–1901, 2012.

10. Sridher, T., A. D. Sarma, P. Naveen Kumar, and K. Lakshmanna, "Results of indoor localization using the optimum pathloss model at 2.4 GHz," *URSI GASS 2020*, 1–4, Rome, Italy, Aug. 29–Sep. 5, 2020.

11. Bultitude, R. J. C., "Measurement, characterization and modeling of indoor 800/900 MHz radio channels," *IEEE Commun. Mag.*, Vol. 25, No. 6, 5–12, Jun. 1987.

12. Sarma, A. D., "The influence of oxygen absorption on frequencies near 60 GHz: A — Review," *IETE Technical Review*, Vol. 5, No. 8, 311–317, 1988, doi: 10.1080/02564602.1988.11438335.

13. Rappaport, T. S., "Characterization of UHF multipath radio propagation inside factory buildings," *IEEE Trans. Antennas Propagat.*, Vol. 37, No. 8, 1058–1069, Aug. 1989.

14. Liu, H., H. Darabi, P. Banerjee, and J. Liu, "Survey of wireless indoor positioning techniques and systems," *IEEE Transactions on Systems, Man, and Cybernetics, Part C (Applications and Reviews)*, Vol. 37, No. 6, 1067–1080, Nov. 2007, doi: 10.1109/TSMCC.2007.905750.

15. Dai, Z. and F. J. Podd, "A power-efficient BLE augmented GNSS approach to site-specific navigation," *2020 IEEE/ION Position, Location and Navigation Symposium (PLANS)*, 1305–1310, Portland, OR, USA, 2020, doi: 10.1109/PLANS46316.2020.9110133.

16. Yu, Y., et al., "Precise 3D indoor localization based on Wi-Fi FTM and built-in sensors," *IEEE Internet of Things Journal*, Vol. 7, No. 12, 11753–11765, Dec. 2020, doi: 10.1109/JIOT.2020.2999626.

17. Zheng, H., X. Zhong, and P. Liu, "RSS-based indoor passive localization using clustering and filtering in a LTE network," *2020 IEEE 91st Vehicular Technology Conference (VTC2020-Spring)*, 1–6, Antwerp, Belgium, 2020, doi: 10.1109/VTC2020-Spring48590.2020.9128821.

18. Aneuryn-Evans, G. and A. Deaton, "Testing linear versus logarithmic regression models," *The Review of Economic Studies*, Vol. 47, No. 1, 1980, 275–291, JSTOR, Accessed Jul. 12, 2020, www.jstor.org/stable/2297113.

19. Christensen, R., *Log-Linear Models and Logistic Regression*, 2 Edition, Springer, 1998.

20. Bendat, J. S. and A. G. Piersol, *Random Data: Analysis and Measurement Procedures*, 4th Edition, Mar. 2010.

21. Zhou, B., Q. Chen, H. Wymeersch, P. Xiao, and L. Zhao, "Variational inference-based positioning with nondeterministic measurement accuracies and reference location errors," *IEEE Transactions on Mobile Computing*, Vol. 16, No. 10, 2955–2969, Oct. 1, 2017, doi: 10.1109/TMC.2016.2640294.

22. Yang, Z. and Y. Liu, "Quality of trilateration: Confidence-based iterative localization," *IEEE Transactions on Parallel and Distributed Systems*, Vol. 21, No. 5, 631–640, May 2010, doi: 10.1109/TPDS.2009.90.

23. Oyie, N. O. and T. J. O. Afullo, "A comparative study of dual-slope path loss model in various indoor environments at 14 to 22 GHz," *2018 Progress in Electromagnetics Research Symposium (PIERS-Toyama)*, 121–128, Toyama, Japan, Aug. 1–4, 2018.

24. Maccartney, G. R., T. S. Rappaport, S. Sun, and S. Deng, "Indoor office wideband millimeter-wave propagation measurements and channel models at 28 and 73 GHz for ultra-dense 5G wireless networks," *IEEE Access*, Vol. 3, 2388–2424, 2015, doi: 10.1109/ACCESS.2015.2486778.

25. Bultitude, R. J. C., P. Melancon, H. Zaghloul, G. Morrison, and M. Prokki, "The dependence of indoor radio channel multipath characteristics of transmit/receiver ranges," *IEEE Journal on Selected Areas in Communications*, Vol. 11, No. 7, 979–990, Sep. 1993, doi: 10.1109/49.233211.

26. Ke, W., J. Jin, H. Xu, K. Yu, and J. Shao, "Online-calibrated CS-based indoor localization over IEEE 802.11 wireless infrastructure," *Progress In Electromagnetics Research C*, Vol. 70, 73–81, 2016.

27. Plets, D., et al., "Coverage prediction and optimization algorithms for indoor environments," *EURASIP Journal on Wireless Communications and Networking*, 1–23, Print, 2012.

28. Whitman, G. M., K.-S. Kim, and E. Niver, "A theoretical model for radio signal attenuation inside buildings," *IEEE Transactions on Vehicular Technology*, Vol. 44, No. 3, 621–629, Aug. 1995, doi: 10.1109/25.406630.

29. ITUR-R P.2040-1, "Effects of building materials and structures on radidowave propagation above about 100 MHz," Jul. 2015.

30. Oyie, N. O. and T. J. O. Afullo, "Measurements and analysis of large-scale path loss model at 14 and 22 GHz in indoor corridor," *IEEE Access*, Vol. 6, 17205–17214, 2018, doi: 10.1109/ACCESS.2018.2802038.

31. Batalhaet, D. S., et al., "Indoor corridor and office propagation measurements and channel models at 8, 9, 10 and 11 GHz," *IEEE Access*, Vol. 7, 55005–55021, 2019, doi: 10.1109/ACCESS.2019.2911866.

32. Su, H. and M. L. Berenson, "Comparing tests of homoscedasticity in simple linear regression," *JSM Math Stat.*, Vol. 4, No. 1, 1017, 2017.

33. Lasla, N., M. F. Younis, A. Ouadjaout, and N. Badache, "An effective area-based localization algorithm for wireless networks," *IEEE Trans. Comput.*, Vol. 64, No. 8, 2103–2118, Aug. 2015.

34. https://www.statisticshowto.com/heteroscedasticity-simple-definition-examples/.

35. http://www.ambrsoft.com/TrigoCalc/Circles2/circle2intersection/CircleCircleIntersection.htm.

36. https://www.espressif.com/sites/default/files/documentation/0a-esp8266ex_datasheet_en.pdf.